RESEARCH ARTICLE

Aggregate WILEY

Tuning interfacial interactions for bottom-up assembly of surface-anchored metal-organic frameworks to tailor film morphology and pattern surface features

Nanoscience: Special Issue Dedicated to Professor Paul S. Weiss

Christine D. Fasana | Fabiola G. Gonzalez | Jonathan W. Wade | Ashley M. Weeks | B. Dulani Dhanapala | Mary E. Anderson ©

Department of Chemistry, Furman University, Greenville, South Carolina, USA

Correspondence

Mary E. Anderson, Department of Chemistry, Furman University, Greenville 29613, SC, USA. Email: maryelizabeth.anderson@furman.edu

Funding information

National Science Foundation - Chemistry Division, Grant/Award Number: 1905221; NSF EPSCoR MADE in SC Program Award, Grant/Award Number: OIA-1655740

Abstract

Surface-anchored metal-organic frameworks (surMOFs) integrate nanoporous supramolecular MOF materials directly into architectures for applications such as gas storage, chemical sensing, and energy storage. Layer-by-layer solution-phase deposition of the MOF-14 components (1,3,5-tris(4-carboxyphenyl)benzene and copper (II) dimers, respectively) produces a porous and conformal film on carboxylterminated self-assembled monolayers (SAMs). In this research, the formation of ultrathin (less than 25 nm) surMOF films on codeposited bicomponent SAMs and microcontact printed SAMs is investigated by atomic force microscopy, ellipsometry, infrared spectroscopy, and contact angle goniometry. SAMs composed of methyl-terminated alkanethiols assembled on gold substrates inhibit surMOF formation, whereas carboxyl-terminated alkanethiols promote MOF-14-based film growth. To tune the density of carboxyl groups that anchor the film, methyl- and carboxylterminated alkanethiols of varying concentrations are codeposited on gold. This systematic study demonstrates how surMOF film formation and morphology are impacted by these SAMs with mixed surface functionalities. Chemical patterning methods for SAMs, such as microcontact printing (μ CP), commonly have mixed chemical functionalities within certain regions of the pattern. Insights gained regarding how mixed surface functionalities affect surMOF film formation are applied herein to optimize the μ CP method to produce chemically patterned SAMs that selectively direct surMOF assembly to produce high-quality surMOF film features.

KEYWORDS

 $atomic\ force\ microscopy,\ microcontact\ printing,\ MOF-14,\ self-assembled\ monolayers,\ surface-anchored\ metal-organic\ frameworks$

1 | INTRODUCTION

Metal-organic frameworks (MOFs) are a class of nanoporous, crystalline materials assembled from metal-based nodes and bridging organic ligands. Research has investigated their viability in a wide range of technologies, such as gas storage, energy conversion, photonics, electronics, sensing, catalysis, and separations.^[1-11] By anchoring an MOF to a surface, the versatility and potential of this high surface area, supramolecular material can be directly integrated into architectures specific to the desired application. ^[12-25]

To produce surface-anchored MOFs (surMOFs) with controlled thickness and surface coverage, films are commonly deposited by introducing the metal ion source and the organic linker in an alternating, sequential, solution-phase deposition process. [12–25] For the incorporation of nanostructured MOFs into device architectures, design rules must be developed that allow for the directed formation of surMOF film structures with regard to patterning features and tailoring morphological parameters, such as film roughness or grain size. Toward the development of these rules to control the structure of surMOF films, this study investigates the impact

This is an open access article under the terms of the Creative Commons Attribution License, which permits use, distribution and reproduction in any medium, provided the original work is properly cited.

 $@\ 2022\ The\ Authors. \textit{Aggregate}\ published\ by\ SCUT,\ AIEI,\ and\ John\ Wiley\ \&\ Sons\ Australia,\ Ltd.$

Aggregate. 2022;3:e241. https://doi.org/10.1002/agt2.241 of modifying the chemical composition of the coating on the substrate that anchors the MOF and explores chemical patterning techniques to selectively direct film formation.

MOF-14 is composed of tritopic ligands and copperpaddlewheel metal nodes with an interwoven pto topology and 1.6 nm pores (Figure S1).[7-10] Alternating solutionphase deposition of MOF-14 components produces ultrathin (<10 nm) conformal films on the underlying substrate, consistent with a van der Merwe (layer-by-layer) thin film growth mechanism.^[25] These films based on the MOF-14 system were anchored to the substrate by a carboxyl-terminated self-assembled monolayer (SAM). The nanoscale morphology, film thickness, and film formation have previously been characterized by atomic force microscopy (AFM). Characterization of the film structure is complicated by the ultrathin film thicknesses investigated (5-20 nm) relative to the unit cell size (a = b = c = 2.7 nm) as well as by the low density of the film because it has high porosity and contains primarily lightweight elements ($Cu_3(C_{27}H_{15}O_6)_2$). The porosity of these MOF-14-based films was previously confirmed by cyclic voltammetry redox probe characterization, and the coordinating chemical functionalities were characterized by infrared (IR) spectroscopy. [25]

The attractive properties of the MOF-14-based film are tunable nanoscale thickness, electrochemical porosity, and the conformal, continuous nature of this surMOF coating on the underlying substrate. These are all useful features for the utilization of an MOF-14-based film in electronic applications, such as a dielectric layer in a transistor or as a solid-state electrolyte layer in thin film batteries. These properties for the MOF-14-based film differ from those observed for other surMOF systems in the literature. [12-24] Typically, surMOF film growth follows a Volmer-Weber growth mechanism with isolated crystallite nucleation and growth that does not continuously coat the underlying substrate until the film is greater than 100-nm thick. Compared to the MOF-14 system, these other surMOF films created by Volmer-Weber growth do not have nanoscale tunability in film thickness; they are considerably thicker, and their morphology is rougher with a higher defect density. Related to the work herein, current research goals in the surMOF field are to understand growth parameters, control or induce film defects, investigate interfacial stability, and develop methods for precise lithography.^[12]

The chemical functionalization of a surface with a SAM is employed to anchor a surMOF to a substrate. SAMs composed of methyl- and carboxyl-terminated alkanethiols have been utilized to inhibit or promote film formation. These molecules spontaneously assemble by solution-phase deposition on gold substrates driven by the strong sulfur-gold bond. Long alkyl chains maximize van der Waals interactions organizing the monolayer, while the tail group of the molecule defines surface properties.^[26-30] These interfacial properties direct the formation of the MOF film deposited by layer-by-layer, solution-phase deposition. Patterned SAMs generated by chemical patterning techniques, such as microcontact printing (μ CP), [28–33] have been used to selectively direct the assembly of surMOF structures onto carboxylterminated regions and inhibit growth on methyl-terminated regions. [14–19] Typically, the chemical regions investigated are greater than 10 μ m in width with surMOF film thicknesses greater than 100 nm, and characterization is done by scanning electron microscopy (SEM), which does not have

the same nanoscale morphological characterization capabilities as AFM. A common challenge associated with chemical patterning, and μ CP especially, is that it is common to have mixed chemical functionalities within certain regions of the pattern. Issues related to this mixing as well as the selectivity and fidelity of the surMOF features have not been carefully studied or discussed in the literature.

In this study, codeposited SAMs and μ CP-patterned SAMs containing methyl- and carboxyl-terminated alkanethiols are investigated as the interfacial coating that anchors the MOF-14-based film to the underlying gold substrate. Characterization of these films was undertaken by ellipsometry, contact angle goniometry (CAG), IR spectroscopy, and AFM. Codeposition of mixed monolayer components tunes surface properties, impacting wetting behavior and tailoring the density of available functional groups that can coordinate with metal ions to promote surMOF growth.[27,34-39] Previous research has shown that solution-phase codeposition of two dissimilar alkanethiols on gold will result in phasesegregation of the two species creating nanoscale (<100 nm) domains.[27,34,35] Motivated by research goals in the sur-MOF field, this study investigates how the codeposited mixed SAMs impact surMOF growth, film defects, and interfacial stability. Additionally, toward the goal of developing precise lithography for surMOFs, the insights gained in this study regarding how the codeposited mixed SAMs impact film formation are applied to improve the directed assembly of MOF-14-based films on μ CP-patterned SAMs with 1- μ m features.

2 | EXPERIMENTAL

2.1 | Materials

For SAM formation and MOF-14 deposition, 16-mercatohexadecanoic acid (MHDA; 90%), 1-octadecanethiol (ODT; 98%), 1,3,5-tris(4-carboxyphenyl)benzene (BTB; 98%) and copper (II) acetate monohydrate (Cu (C₂H₃O₂)₂•H₂O; 98%) were purchased from Sigma-Aldrich. Ethanol (200 proof, ACS/USP grade) was solvent for all solutions and purchased from Pharmco by Greenfield Global. Gold-coated (100 nm) silicon wafers with an adhesive titanium layer (5 nm) were utilized as substrates and purchased from Platypus Technologies. To fabricate stamps, a Sylgard 184 Sillicone Elastomer Kit was purchased from Dow Silicones Corporation.

2.2 \mid Gold substrate functionalization with SAMs

SAMs were fabricated to anchor the MOF film to the substrate. Gold substrates were submerged in a 1-mM ethanolic solution composed of MHDA and/or ODT for 1 h. For the formation of these mixed SAMs, MHDA and/or ODT were codeposited from 1-mM ethanolic solutions. The composition of ODT was 0%, 25%, 50%, 75%, and 100% with MHDA as the remaining percentage of the concentration. Note that these percentages do not quantitatively reflect the composition of the molecules on the substrate, but these percentages will be used to describe the substrates through-

out this discussion. Then, substrates were removed from the solution, rinsed with ethanol, and dried using nitrogen gas.

2.3 | Patterning gold substrate with SAMs

To fabricate polydimethylsiloxane (PDMS) stamps for μ CP to generate chemical patterns of SAMs, a 1:10 mass ratio of curing agent to base was mixed.[31-33] Air bubbles were removed under vacuum from the mixture before and after it was poured over a CD master used to template linear structures into the PDMS. The PDMS was cured in a vacuum oven at ~60°C for 1 h. After the stamp was removed from the master template, it underwent a cleaning process to eliminate low molecular weight species. This was done by immersing the stamp in hexanes with sonication for 30 min and then heating it under vacuum at $\sim 100^{\circ}$ C for 1 h. Next, the stamp was immersed in a 50:50 solution of DI (deionized) water and ethanol with sonication for 30 min, removed from the solution, and then heated for an hour at ~60°C. This process of stamp cleaning with hexanes and then DI water:ethanol mixture was repeated three times.

For the μ CP procedure, [31–33] ethanolic solutions of 1-mM MHDA or ODT were used as ink and backfill solutions. The surface of the PDMS stamp was coated with the ink solution (ODT or MHDA) for 1 min and then dried using nitrogen gas. The stamp was then placed onto the gold substrate with a weight of four quarters added to the back of the stamp. The substrate was in contact with the stamp for 1 min. After the stamp was removed, the substrate was immediately immersed in the backfill solution (MHDA or ODT) for 10 min. Then, the substrate was rinsed with ethanol and dried with nitrogen gas.

2.4 | Deposition of MOF components for film formation

According to the literature precedent, [25] thin films based on the coordination of MOF-14 were fabricated on SAM-functionalized gold substrates using alternating, solution-phase deposition of the inorganic and organic components. An automated deposition system, the Midas III-Plus Automated Slide Stainer, was employed to deposit these MOF components. SAM-functionalized Au substrates were submerged for 30 min in a 1-mM ethanolic solution of $\text{Cu}(\text{C}_2\text{H}_3\text{O}_2)_2 \cdot \text{H}_2\text{O}$. Then, the substrates were submerged in a 0.1-mM ethanolic solution of BTB for 1 h. Between the deposition of each inorganic and organic component, substrates were rinsed in ethanol for 5 min and dried at 30°C for 10 min. The process was repeated for the desired number of deposition cycles.

2.5 | Ellipsometry

Before and after SAM formation as well as following each set of four MOF deposition cycles, ellipsometry characterization was conducted using a single wavelength, fixed angle LSE Stokes Ellipsometer (Gaertner Scientific Corporation). Film thickness data were obtained using a helium-neon laser with a wavelength of 6328 Å at a fixed incidence angle of 70°. A minimum of six spots per sample were collected, and at

least two replicates for each sample type were investigated. Film thickness was calculated via GEMP analysis software using values of 1.5 and 0 for the index of refraction and the extinction coefficient, respectively. [23,24,30]

2.6 | CAG

Following both SAM formation and MOF deposition, the surface properties were investigated via CAG. A KSV Theta Optical Tensiometer collected static contact angle data with 5 μ l drops of DI water delivered. An LED camera took images at a resolution of 512 × 480 pixels, and Attension Theta software measured the contact angle for the left and right sides of each droplet. For each sample type, a minimum of three drops per sample were investigated with a minimum of two replicates.

2.7 | IR spectroscopy

After film deposition, IR spectra were collected from 4000–6000 cm⁻¹ in attenuated total reflectance mode using a PerkinElmer Spectrum Two Fourier transform IR spectrometer. All spectra were collected with a resolution of 4 cm⁻¹ over a set of 64 scans, and a bare gold substrate was used as the background.

2.8 | AFM

Substrates were characterized via AFM following surMOF deposition to investigate film morphology. Three images (256 \times 256 pixels) were taken at three different locations for each sample at 2.5 \times 2.5 μm using an NX10 AFM (Park Systems). Images were obtained in noncontact mode using a Park Systems PPP-NCH 10 M probe (42 N/m force constant). SmartScan data acquisition software was employed with a 1-Hz scan rate and 10-nm setpoint. The XY scanner was a single module flexure with a closed control and a scan range of 50 μm by 50 μm . Images analyzed with XEI AFM data analysis software (Park Systems) were employed to quantitatively investigate surface morphology, specifically surface roughness (Rq). The average Rq values and standard deviations presented are representative of at least two sample replicates and a minimum of three spots per sample.

3 | RESULTS AND DISCUSSION

To better understand surMOF growth, defects, stability, and patterning, this research investigates MOF-14-based films assembled on codeposited bicomponent SAMs and μ CP-patterned SAMs. Substrates with codeposited mixed SAMs composed of ODT and MHDA (0%, 25%, 50%, 75%, and 100% ODT) were characterized by ellipsometry, CAG, IR, and AFM before and after four deposition cycles of MOF-14. Additional cycles of MOF deposition on the 0%, 25%, and 50% ODT codeposited SAMs were conducted to determine how morphological features (i.e., surface roughness, defects) propagated. Based on findings from the codeposited mixed SAMs, two approaches for patterning monolayers of ODT and MHDA by μ CP were examined. The difference between the approaches is the compound used for stamping

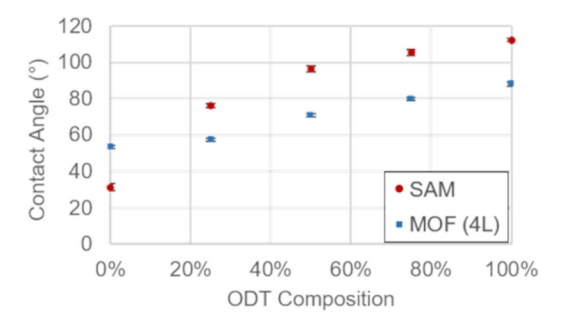


FIGURE 1 Contact angle goniometry was used to investigate the wetting properties of substrates before (self-assembled monolayer [SAM]) and after four layer-by-layer deposition cycles (metal-organic framework [MOF; 4L]). Average contact angles measured with standard deviation values are plotted as a function of octadecanethiol (ODT) % composition utilized in the 1-mM ethanolic solution to compose the SAM. Note that the remaining composition of the SAM was composed of 16-mercaptohexadecanoic acid (MHDA)

and the compound used to backfill the unpatterned region. The compound used as the backfill will typically become a minor component mixed within the stamped compound region. Comparison of MOF deposition on these patterned SAMs further elucidated the impact of mixed monolayers on directed selective film formation and identified an optimized process for high-quality patterning of surMOFs.

3.1 | Early stages of film growth on codeposited monolayers

Mixed monolayers formed by codeposition of ODT and MHDA were investigated before and after MOF-14 deposition. CAG allows us to confirm that the content of the mixed SAM effectively impacts the wetting properties, as would be anticipated due to the increased incorporation of a methylterminated alkanethiol (ODT) with the carboxyl-terminated alkanethiol (MHDA). Figure 1 contains CAG data for the codeposited mixed SAMs before and after the deposition of MOF-14 components. After the formation of the SAM, the 0% ODT SAM (100% MHDA) is hydrophilic with a contact angle of 31 \pm 2°, in contrast to the 100% ODT SAM with a hydrophobic contact angle of $112 \pm 1^{\circ}$. For the SAMs made from 25%, 50%, and 75% ODT composition solutions, contact angles fall appropriately within the aforementioned bounds (76 \pm 1, 96 \pm 2, and 105 \pm 2°, respectively). These data confirm that monolayers of mixed compositions are formed with increasing hydrophobicity reflective of the increasing ODT content within the codeposition solution, which is consistent with reported values in the literature. [36] Previous research showed preferential adsorption of ODT from solution onto a gold substrate that resulted in an ODTenriched mixed SAM. [37–39] For all mixed SAMs, an average height of ~18 Å was measured by ellipsometry, suggesting a uniform monolayer. After four deposition cycles of MOF-14 components, CAG values for the films formed on the 0% and 25% ODT substrates are similar (53 \pm 1 and 57 \pm 1°, respectively). Films on the other samples demonstrate higher contact angles (71 \pm 1, 80 \pm 1, and 88 \pm 1° for 50%, 75%, and 100% ODT, respectively). These CAG findings for the films on the SAMs with higher ODT content suggest that ODT regions may be exposed and impact surface hydrophobicity. Additionally, films with higher roughness values will have increased contact angles due to the pinning effect. AFM imaging will elucidate if the increasing ODT content results in rougher films.

AFM images collected after four deposition cycles of MOF-14 components on the codeposited SAMs are presented in Figure 2 along with associated film roughness values, ellipsometric thicknesses, and graphics representing the gold substrate, SAM, and film structure. Figure 2A is for the MOF-14 film on the pure MHDA SAM (0% ODT), revealing a conformal film morphology that is consistent with the underlying gold grain structure of the substrate (see Figures S2 and S3 for AFM images enlarged with annotation highlighting morphological features). The average roughness values before and after film growth are both 2.1 ± 0.4 nm. After film growth, ellipsometry showed an average film thickness of 87 Å. An IR spectrum (Figure S4) collected for the film deposited on the 0% ODT substrate is consistent with previous findings.^[25] In contrast, Figure 2E is for the MOF-14-based film on the pure ODT SAM (100% ODT), which has only isolated protrusions of nonspecific binding. The average roughness value after MOF deposition $(3.1 \pm 0.2 \text{ nm})$ increased relative to the 0% ODT sample due to these small protrusions that formed. For this 100% ODT sample, ellipsometry showed an average film thickness increase of \sim 5 Å after four deposition cycles, which is likely due to adventitious binding during the solution-phase deposition process. The IR data for 100% ODT (Figure S4) demonstrated a very low peak intensity as a minuscule amount of film was formed, which is consistent with the AFM and ellipsometry data. The ODT SAM inhibited the formation of the MOF-14based film, which was significantly different from the amount of film growth on the MHDA SAM. These results for the 0% and 100% ODT substrates are consistent with previously published findings.^[25]

The AFM image for the MOF-14-based film on the 25% ODT codeposited SAM shows a morphology similar to that of the 0% ODT SAM (Figure 2B). For both the 0% and 25% ODT samples, the grain structure of the underlying gold is prominently visible. A subtle difference for the 25% ODT sample is observed in that these grains appear more textured. This observed difference is likely due to the underlying SAM for the 25% ODT sample not being a continuous coating of carboxyl termination and instead containing methyl-terminated domains (or defects) that do not promote film growth. The texture observed in the AFM images for the 25% ODT sample did not impact the overall film roughness, as the average roughness value for the 25% ODT sample (2.2) \pm 0.1 nm) does not differ from that of the 0% ODT sample. The similarity of the CAG values for MOF-14-based films on the 0% and 25% ODT suggests that both samples have conformal coatings with none of the underlying SAM exposed. For the 25% ODT sample, the average film thickness (70 Å) and the intensity of the IR signal collected (Figure S4) are both slightly less in comparison to the 0% ODT sample. After four cycles of MOF-14 deposition, the film deposited on the 25% ODT SAM was minimally impacted by the incorporation of the methyl-terminated molecule, suggesting that the initial formation of the MOF-14-based film tolerates the incorporation of nonbinding surface groups.

The morphology of the film on the 50% ODT SAM observed by AFM in Figure 2C is distinctly different from the

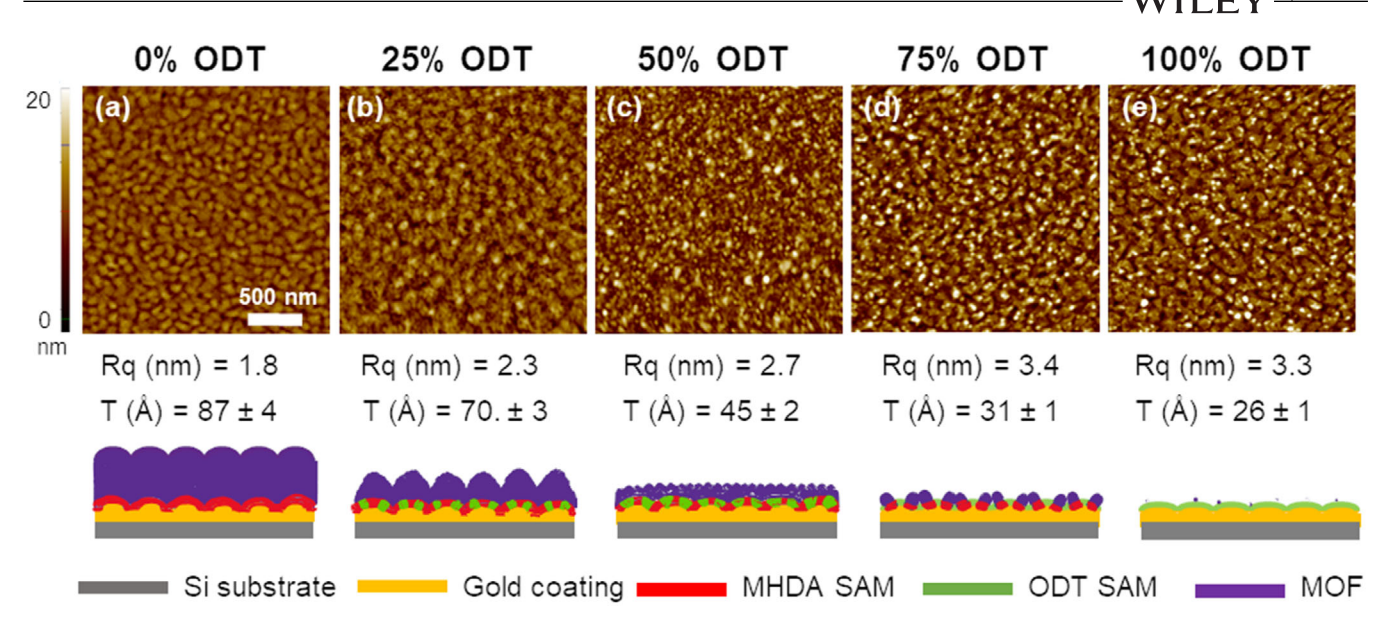


FIGURE 2 Representative atomic force microscopy (AFM) images $(2.5 \times 2.5 \,\mu\text{m})$ collected after film growth of MOF-14-based films anchored to Au substrates via mixed concentrations of carboxyl- and methyl-terminated SAMs, respectively MHDA and ODT. Prior to four cycles of MOF deposition, SAMs were formed for 1 h from 1-mM ethanolic solutions, which were composed of the indicated amount of ODT indicated above each image. Below each image, the corresponding surface roughness values (Rq) and the average MOF-14 thicknesses (T) and associated standard deviations as determined by ellipsometry are provided. Graphics are included to demonstrate a proposed side-view perspective of MOF-14 growth to complement the AFM images with the top-down perspective

0% and 25% ODT samples because the gold grain structure is not observed. Thus, the film on the 50% ODT sample does not conform with the underlying substrate. This film morphology has small bulbous features that produce an increased average roughness of 3.0 ± 0.2 nm, which is reflective of this different film structure. The bulbous rough texture of the film on the 50% ODT SAM is likely templated by the phasesegregated SAM domains in which the MHDA domains will be nucleation sites for film formation. The film thickness (45 Å) by ellipsometry is approximately half that of the 0% ODT substrate, and a comparatively lower IR signal is observed (Figure S4). A significant difference in film formation and morphology is observed with this 50% ODT surface coating. This reveals how the mixed chemical functionalities produced by the codeposited 50% ODT sample are a growth parameter that allows film morphology and structure to be tailored. Additionally, the SAM coating with a mixture of chemical domains could be described as providing sites at the interface that both nucleate film growth or induce defects resulting in a distinctive film morphology. The contact angle for these 50% samples is higher than that for the 0% and 25% substrates, which is likely due to the increased surface roughness and may also indicate that there are small regions of hydrophobic ODT SAM exposed at the interface. The findings here for the 50% ODT sample illuminate a growth parameter that can be tuned to produce a rougher film, which may be desirable for applications in which a high surface area is valuable.

The AFM image in Figure 2D for the 75% ODT substrate after four deposition cycles of MOF-14 reveals a gold grain structure with small protruding regions of deposited film. More of these protrusions are observed on this sample relative to the 100% ODT sample. Based on previous research, [34,35] the SAM structure for the 75% ODT sample contains nanoscale MHDA regions surrounded by ODT. The MOF-14-based film coordinates and grows primarily on these isolated MHDA regions, which results in this substrate hav-

ing the highest average surface roughness of 3.6 ± 0.2 nm. The average film thickness (31 Å) and IR peak intensities are slightly higher than those of the 100% ODT sample (Figure S4). After four deposition cycles, the contact angle for the film deposited on the 75% ODT sample is similar to the 100% ODT. These CAG data are consistent with AFM, which shows gold grains coated with ODT and small regions of deposited MOF-14-based film bound to the MHDA regions.

For directed bottom-up assembly of surMOFs on chemically patterned features, it is desirable to have MHDA regions that promote MOF growth and ODT regions that inhibit growth. The 100% ODT samples are effective for the inhibition of MOF film formation. For the 75% ODT sample, when MHDA is a minor component mixed with the ODT, the capability of the SAM to inhibit MOF film growth is compromised significantly. Thus, this shows that it is problematic if MHDA is mixed in as a minor component with ODT. However, when ODT is mixed in as the minor component with MHDA (25% ODT sample), a conformal MOF-14-based film is found to continuously coat the substrate with minimal differences in thickness and morphological features relative to the film formed on the 0% ODT sample. The implications of these findings will be further explored in MOF Film Growth on μ CP Patterned Monolayers section.

3.2 | Evolution of film morphology on codeposited monolayers with continued deposition

In the first part of the study, the investigation of the initial film formation after four deposition cycles of MOF-14 revealed that codeposited bicomponent SAMs on the surMOF are a growth parameter to control surMOF film morphology and defect density. The next part of the study investigates surMOF formation on 0%, 25%, and 50% ODT SAMs

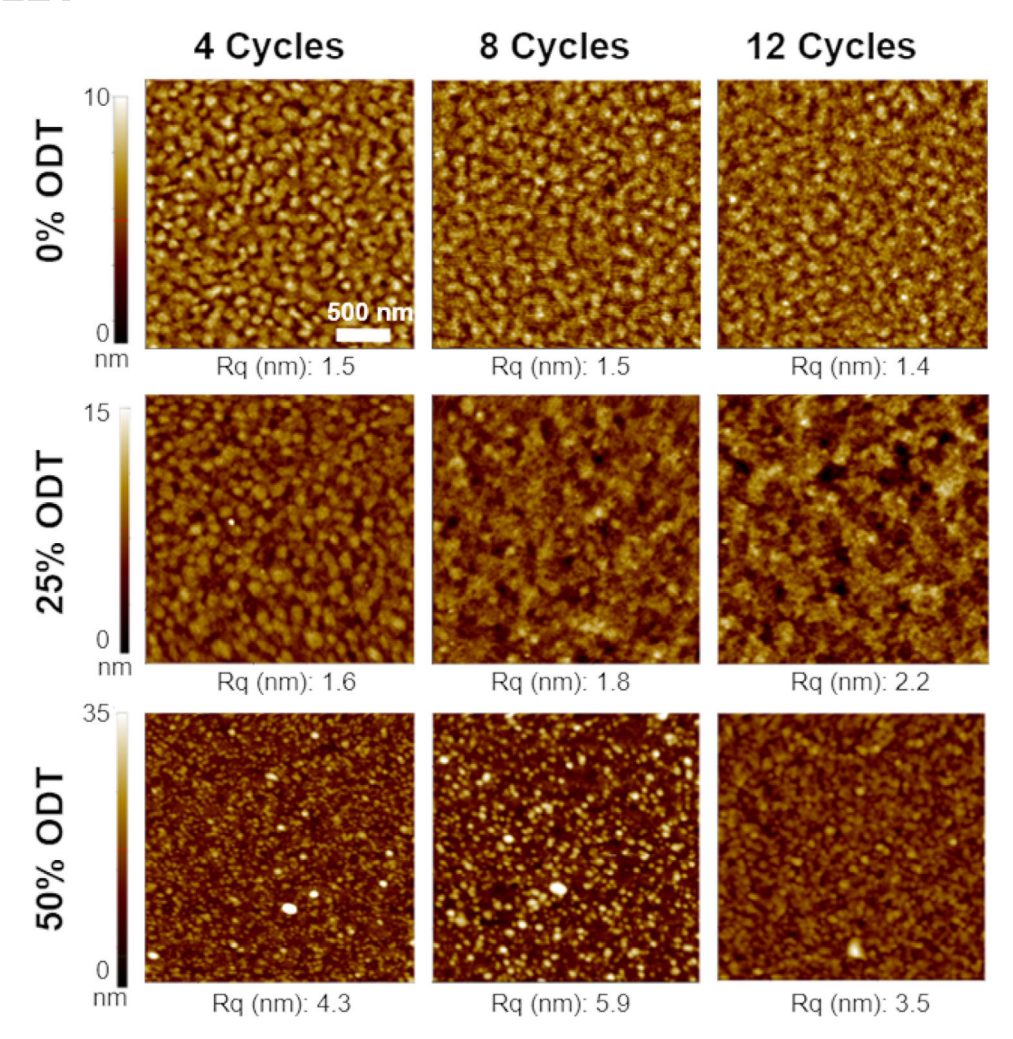


FIGURE 3 Representative AFM images $(2.5 \times 2.5 \,\mu\text{m})$ collected after four, eight, and 12 cycles of layer-by-layer film deposition to generate MOF-14-based films. The MOF was anchored to Au substrates coated with a SAM produced by a 1-mM ethanolic solution containing 0%, 25%, and 50% methyl-terminated alkanethiol (ODT), with the remainder of the composition being a carboxyl-terminated alkanethiol (MHDA). Below each image, the associated surface roughness values (Rq) are given

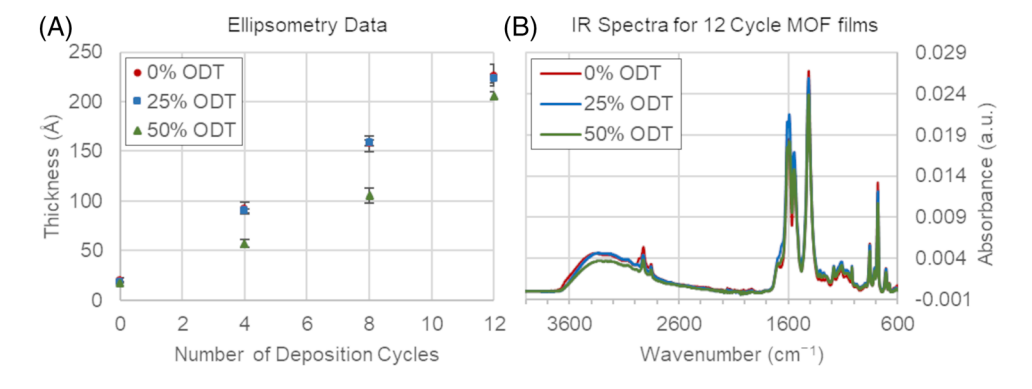


FIGURE 4 Films deposited on three different SAM compositions are characterized by (A) ellipsometry and (B) infrared (IR) spectroscopy. The SAM composition is shown in the legend as % ODT. Note that the solution from which the SAM was formed included the indicated amount of ODT, and the remaining percentage of the 1 mM solution was composed of MHDA. (A) MOF film thickness as determined by ellipsometry with average thicknesses and associated standard deviation values plotted as a function of the number of deposition cycles. (B) IR spectra after 12 MOF deposition cycles on these three different SAM compositions

and how differences in morphology and defects propagate after additional deposition cycles of MOF-14 components. Subtle morphological differences were observed by AFM for films deposited on the 0% ODT, compared to the 25% ODT samples, while significant differences were found for 50% ODT samples (first column, Figure 3). The ellipsometry data

in Figure 4A show that the film thickness on the 50% ODT sample is significantly less than the film thicknesses on the 0% and 25% ODT SAMs.

The film morphology on the 0%, 25%, and 50% ODT SAMs after eight deposition cycles is shown in the second column of Figure 3. The morphologies of all three samples

are now distinctly different. While the film morphology on the 0% and 50% ODT SAMs is preserved from deposition cycles four to eight, a change in morphology for the film on the 25% ODT SAM is observed. The underlying gold grain structure is no longer prominent for the film on the 25% ODT SAM following these additional deposition cycles. Ellipsometry data (Figure 4A) again reveal that the film thickness on the 25% ODT SAM is consistent with that on the 0% ODT sample. The thickness of the film on the 50% ODT SAM increases from four to eight cycles, but it is still significantly less than that on the 0 and 25% ODT samples.

Images obtained by AFM of films formed after 12 deposition cycles of MOF-14 components on 0%, 25%, and 50% ODT SAMs are shown in the third column of Figure 3. These three samples have different morphologies from each other just as they did after eight deposition cycles. While films formed on the 0% and 50% ODT SAMs have consistent features produced from four through 12 deposition cycles, the film on the 25% ODT SAM does not. For the film on the 25% ODT SAM, the morphology changes from a conformal film that matches the underlying gold cobblestone structure (after four deposition cycles) to a film that is slightly rougher with smaller features and some long-range undulations (after eight and 12 deposition cycles). While the morphology evolves, the average roughness values for the 25% ODT samples do not change significantly after four, eight, and 12 cycles of deposition (2.2 \pm 0.1 nm, 2.1 \pm 0.1 nm, and 2.4 \pm 0.6 nm, respectively). The film morphology of the 50% ODT sample is consistent throughout the 12 deposition cycles. Bulbous features observed after four deposition cycles are due primarily to MOF film growth formed on MHDA SAM domains that result from the codeposition solution. [34,35] The rough texture of the film on the 50% ODT SAM, potentially templated by MHDA SAM domains, propagates after eight and 12 deposition cycles with roughness values of 4.1 \pm 0.5 nm and 5.7 \pm 0.2 nm, respectively.

For films deposited on the 0% and 25% ODT samples, film thickness increases after 12 deposition cycles were again within error of one another (Figure 4A). Throughout the film formation for both the 0% and 25% ODT SAM, the film thickness increased in a linear manner, consistent with the conformal and smooth morphology observed by AFM. Linear fit for both samples resulted in a slope of 17 Å per deposition cycle with an R^2 value of 0.999 (Figure S5). The film thickness on the 50% ODT SAM is initially significantly less than that on the 0% ODT. The change from zero to four cycles is \sim 25 Å for the 50% ODT and \sim 65 Å for the 0% ODT (Figure 4A). The change in thickness determined by ellipsometry for films on 50% ODT SAMs was \sim 25 Å, \sim 50 Å, and ~100 Å as the film went from zero to four, then four to eight, and then eight to 12 deposition cycles (Figure 4A). This nonlinear film thickness increase is likely due to increased surface roughness and associated increased surface area, permitting additional MOF film growth. This increase was such that the thickness of the 50% ODT sample was similar to that of the 0% and 25% ODT films after 12 deposition cycles. The IR spectra for all of these samples after 12 deposition cycles show similar absorption bands to one another (Figure 4B) and to the previously published IR data for these MOF-14based films. [25] These IR data support that the films formed in this study have the same coordination environment as those previously investigated. These highly porous films with

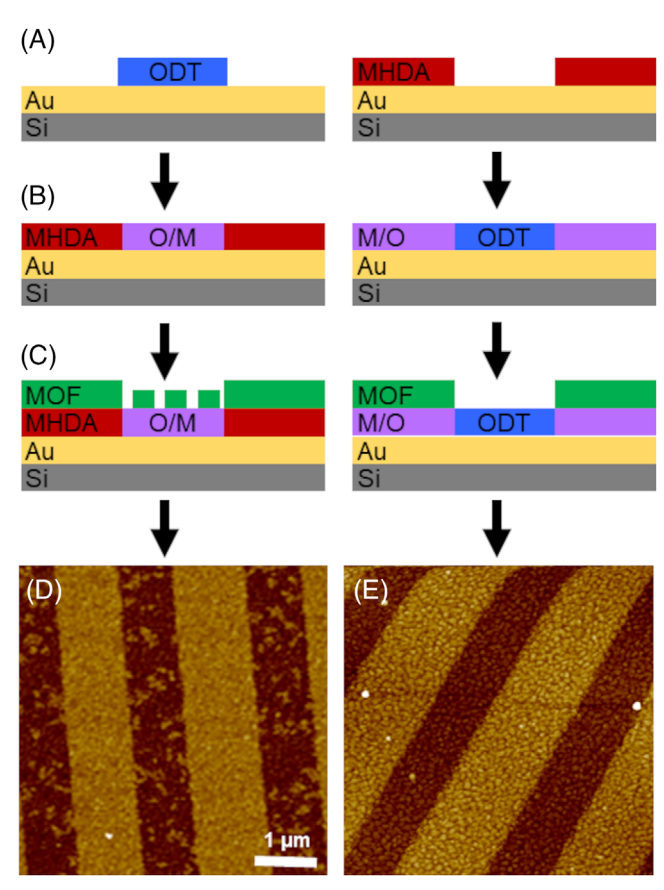
thicknesses less than 25 nm (<10 MOF-14 unit cells) cannot be characterized by routine X-ray diffraction, and future research would require advanced X-ray scattering techniques to further understand the structure of the MOF-14-based thin films studied herein.

Propagation of the film morphology throughout the film deposition cycles was found to occur on the 0% and 50% ODT SAMs, whereas the film morphology on the 25% ODT SAM evolved after the initial formation of the initial four layers. All three of these SAM compositions had uniquely different morphologies observed by AFM with a consistent chemical structure by IR. These findings demonstrate that the composition of the SAM anchoring the surMOF to the substrate can be utilized as a growth parameter to influence film morphology and roughness. The inclusion of methyl-terminated alkanethiols with carboxyl-terminated alkanethiols to produce SAMs can be used to tailor film morphology and engineer defects to tune surMOF structures and properties.

3.3 | MOF film growth on μ CP-patterned monolayers

Toward the goal of developing and optimizing lithographic methods to pattern surMOFs, the findings associated with sur-MOF growth on codeposited SAMs are applied to optimize the selective directed assembly of MOF-14-based films on 1- μ m SAM features patterned by μ CP. Chemically patterned SAMs composed primarily of ODT or MHDA regions have been utilized to direct the assembly of surMOF films inhibiting and promoting film growth.[14-19] Previous research surveyed surMOFs formed by this method primarily utilizing SEM and typically investigating surMOF film thicknesses greater than 100 nm on chemically patterned SAM features that are $10-100 \, \mu \text{m}$ in width. [15-19] The investigation herein regarding surMOF growth on codeposited SAMs is especially relevant for directed surMOF assembly on μ CP-patterned SAMs because the initially patterned chemical region often has some of the secondary component mixed within during the exposure of the sample to the secondary chemical component.

μCP is an additive, bottom-up method for chemically patterning substrates that uses elastomeric PDMS stamps to fabricate micro- and nanoscale features. To begin this soft lithography process, the stamp has raised and recessed patterns that are coated with molecular solutions (e.g., SAMbuilding alkanethiols), referred to as the ink. Stamp contact with the gold substrate selectively transfers the pattern from the raised features on the stamp to the substrate. Then, this gold substrate with a patterned alkanethiol region is exposed to a secondary alkanethiol that forms a SAM in unpatterned gold regions, which is referred to as the backfill process.[31-33] Note that the initial component patterned by the stamp is exposed to the secondary component that backfills unstamped regions. Thus, while the regions composed of the backfilled molecules are pure-phase, the stamped regions are typically composed of the initial component with small amounts of the secondary component mixed within. [31-33] The extent of this mixture is based on the stability of the initial component relative to the secondary.[40-42]



F1GURE 5 A graphic with a proposed side-view perspective of microcontact printing (μ CP)-patterned SAMs and subsequent MOF-14 growth. (A) Substrate patterned by μ CP with the initial SAM component stamped (ODT, shown in blue, is patterned first in the left column, and MHDA, shown in red, is patterned first in the right column). (B) Next, the unpatterned regions are backfilled with the other component. Note that this creates mixed SAMs when the backfill molecule intercalates with the initially stamped molecule (this mixed region is purple and denoted O/M on the left and M/O on the right) and that the backfilled regions of the pattern are pure-phase. (C) After four deposition cycles of MOF-14 components, MOF film coverage is depicted as observed by microscopy. (D) Representative AFM images (5 x 5 μ m), which were collected after film growth of MOF-14-based films anchored to Au substrates patterned with ODT and MHDA as depicted in the schematics above

For this study, the initial μ CP approach patterned substrates with ODT as the ink and MHDA as the backfill molecule. This is the common approach because the hydrophobic and/or longer-chain molecule will diffuse less when stamped and produce high fidelity patterns relative to the PDMS stamp. PDMS stamp features were 1-\mu wide linear structures, so lines of ODT ink were transferred by contact between the stamp and substrate with open regions between ODT lines backfilled with MHDA. After four deposition cycles on the patterned substrate, bright lines are observed in the AFM image (Figure 5A), representing MHDA regions on which conformal MOF growth protrudes from the substrate. Lower lying regions, which appear dark in the image, between these MOF lines contain bright protrusions randomly distributed. These protrusions occur in regions where ODT was stamped onto the substrate. MHDA molecules likely intercalate and mix within ODT regions during the backfill process in sufficient amounts to promote MOF growth.

The next approach to improve MOF pattern quality was to use MHDA as ink and ODT as backfill. This resulted in a difference in selective surMOF formation observed by AFM (Figure 5B). Bright lines protruding from the surface are observed with low-lying dark regions between. Note that these dark regions do not contain irregular bright protrusions as observed when ODT was the ink. A few random bright protrusions are found on both the MHDA and ODT regions, which is likely due to adventitious substances nonspecifically bound during solution-phase deposition.

The difference in stamping with ODT versus MHDA ink is unlikely to produce highly disparate quality patterns because ODT backfill is unable to intercalate within MHDA stamped regions. Instead, it is probable that MOF growth on MHDA regions tolerates the small percentage of ODT that is incorporated (likely less than the 25% ODT composition discussed in the mixed monolayer section). Conversely, ODT-stamped regions with intercalated MHDA molecules were not sufficiently able to inhibit MOF growth. Thus, in the case of the MHDA ink and ODT backfill sample shown in Figure 5B, ODT successfully inhibited MOF growth so that there were no bright protrusions between the bright lines of MOF growth.

4 | CONCLUSION

This research investigated MOF-14-based film growth on different SAM compositions, titrating in non-coordinating ODT with coordinating MHDA to see how this change in the anchoring layer affects growth parameters, defects, and interfacial stability. These findings were then used to improve lithographic methods to pattern high-quality surMOF features. Investigation of codeposited SAMs anchoring the film highlighted the durability of surMOF formation with limited amounts of coordinating functional groups and demonstrated how these mixed codeposited SAMs can tailor the resulting morphology of the surMOF film. Throughout 12 deposition cycles, the surMOF film thicknesses of the 0% and 25% ODTs were the same at a rate of 17 Å of film deposited per cycle, which is similar to previous findings for MOF-14-based films.^[25] For the film deposited on the 25% ODT SAM, a conformal morphology similar to that of the 0% ODT sample was observed after the foundational first four deposition cycles. Subsequent film deposition on the 25% ODT SAM resulted in a changed film morphology that no longer displayed conformity with the underlying gold substrate. This is likely due to the propagation of defects induced by the noncoordinating ODT in the anchoring SAM. The MOF-14-based film on the 50% ODT SAM had a rough film morphology that did not conform with the underlying gold substrate after the initial four deposition cycles, and this surface texture was consistent throughout the 12 deposition cycles. While the amount of film deposition shown by ellipsometry was initially less on this 50% ODT SAM when compared to the 0% and 25% samples, the rate of film deposition increased such that after 12 deposition cycles, the difference was minor. Future research will investigate how the film morphology of surMOFs formed by Volmer-Weber, such as HKUST-1, is impacted by anchoring SAMs composed of mixed surface functionalities. To verify that other surMOFs formed by van der Merwe behave in the same manner as MOF-14, the deposition of MOF-399 will be investigated. Surface morphology is a key feature to tailor for the incorporation of surMOFs into architectures for gas

storage or devices for energy storage. For gas adsorption or sensing technologies, a rough film with a high surface area is desirable, whereas electronic devices containing surMOFs as dielectric or conducting layers would need conformal films without defects.

To lithographically pattern surMOF structures, directed bottom-up assembly of the film on chemically patterned SAMS created by μ CP has been demonstrated. This soft lithography method has an initial component pattern followed by a subsequent exposure that fills in unpatterned regions. Thus, mixing by intercalation occurs in those initial regions, which could impact the effectiveness of selective MOF film formation. Our systematic study showed that sur-MOF growth can tolerate small amounts of noncoordinating surface functionalities (ODTs) mixed with coordinating ligands (MHDA). Small amounts of coordinating ligands mixed with noncoordinating ligands, however, will induce MOF formation nucleated from those coordination sites. The selection of which chemistry is patterned first has been herein shown to significantly impact the selectivity of the surMOF growth. High-quality surMOF features patterned on the 1um scale were obtained by patterning first with the MHDA and then subsequently with ODT. The ODT that likely intercalates in the MHDA regions does not affect the surMOF film quality, and the regions of the substrate that were not patterned by MHDA contain pure ODT that successfully inhibits film growth. In contrast, surMOF growth outside of the desired patterned regions problematically occurs when ODT is patterned first and MHDA intercalates within it. This optimization of the patterning process is pertinent to improve pattern fidelity for surMOF films that form via van der Merwe or Volmer-Weber growth mechanisms, as the selectivity of the film growth, in both cases, is dependent on the anchoring SAM composition. This investigation reveals the fundamentals of the anchoring SAM in determining film growth, surface morphology, defect propagation, and interfacial stability, and based on these findings, strategies were implemented to fabricate high-quality lithographically defined surMOF films.

ACKNOWLEDGMENTS

Aspects of this work were supported by NSF-CHE 1905221, NSF EPSCoR MADE in SC Program Award #OIA-1655740, the Henry Dreyfus Teacher-Scholar Award (MEA), the Arnold and Mabel Beckman Foundation Scholars Program (CDF), as well as funding from Furman University and the Chemistry Department. The authors have no conflicts of interest to declare.

CONFLICT OF INTEREST

The authors declare that there is no conflict of interest that could be perceived as prejudicing the impartiality of the research reported.

ETHICS STATEMENT

This data was collected and analyzed in an ethical manner. No animal or human subject studies were involved in this research.

DATA AVAILABILITY STATEMENT

Data associated with the findings of this study are available from the corresponding author upon reasonable request.

ORCID

Mary E. Anderson https://orcid.org/0000-0001-8369-2177

REFERENCES

- R. Freund, O. Zaremba, G. Arnauts, R. Ameloot, G. Skorupskii, M. Dincă, A. Bavykina, J. Gascon, A. Ejsmont, J. Goscianska, M. Kalmutzki, U. Lächelt, E. Ploetz, C. S. Diercks, S. Wuttke, *Angew. Chem. Int. Ed.* 2021, 60, 23975.
- L.S. Xie, G. Skorupskii, M. Dincă, Chem. Rev. 2020, 120, 8536.
- J. Fonseca, T. Gong, L. Jiao, H. -L. Jiang, J. Mater. Chem. A. 2021, 9, 10562.
- L. E. Kreno, K. Leong, O. K. Farha, M. Allendorf, R. P. Van Duyne, J. T. Hupp, *Chem. Rev.* 2012, 112, 1105.
- 5. A. Dhakshinamoorthy, H. Garcia, Chem. Soc. Rev. 2014, 43, 5750.
- B. Li, M. Chrzanowski, Y. Zhang, S. Ma, Coord. Chem. Rev. 2016, 307, 106.
- B. Chen, M. Eddaoudi, S. T. Hyde, M. O'Keeffe, O. M. Yaghi, *Science* 2001, 291, 1021.
- H. Furukawa, Y. B. Go, N. Ko, Y. K. Park, F. J. Uribe-Romo, J. Kim, M. O'Keeffe, O. M. Yaghi, *Inorg. Chem.* 2011, 50, 9147.
- J. R. Karra, B. E. Grabicka, Y. -G. Huang, K. S. Walton, J. Colloid Interface Sci. 2013, 392, 331.
- X. Zhao, C. Xin, X. Tian, Y. Li, W. Bian, P. Lian, Adsorp. Sci. Technol. 2012, 30, 483.
- K. Taylor-Edinbyrd, T. Li, R. Kumar, *Phys. Chem. Chem. Phys.* 2017, 19, 11947.
- A. L. Semrau, Z. Zhou, S. Mukherjee, M. Tu, W. Li, R. A. Fischer, *Langmuir* 2021, 37, 6847.
- 13. J. Liu, C. Wöll, Chem, Soc. Rev. 2017, 46, 5730.
- O. Lugier, N. Thakur, L. Wu, M. Vockenhuber, Y. Ekinci, S. Castellanos, ACS Appl. Mater. Interfaces 2021, 13, 43777.
- J. Zhaung, A. Terfort, C. Wöll, Coord. Chem. Rev. 2016, 307, 391.
- O. Shekhah, H. Wang, S. Kowarik, F. Schreiber, M. Paulus, M. Tolan, F. Sternemann, C. Evers, D. Zacher, R. A. Fischer, C. Wöll, *J. Am. Chem. Soc.* 2007, 129, 15118.
- C. Munuera, O. Shekhah, H. Wang, C. Wöll, C. Ocal, *Phys. Chem. Chem. Phys.* 2008, 10, 7257.
- Z. -G. Gu, A. Pfriem, S. Hamsch, H. Breitwieser, J. Wohlgemuth, L. Heinke, H. Gliemann, C. Wöll, Micropor. Mesopor. Mat. 2015, 211, 82.
- J. J. Gassensmith, P. M. Erne, W. F. Paxton, C. Valente, J. F. Stoddart, Langmuir 2011, 27, 1341.
- O. Shekhah, H. Wang, D. Zacher, R. Fischer, C. Wöll, *Angew. Chem. Int. Ed.* 2009, 48, 5038.
- H. N. Rubin, B. H. Neufeld, M. M. Reynolds, ACS Appl. Mater. Interfaces 2018, 10, 15189.
- T. P. Vello, M. Strauss, C. A. R. Costa, C. C. Corrêa, C. C. Bof Bufon, *Phys. Chem. Chem. Phys.* 2020, 22, 5839.
- Redel, Z. Wang, S. Walheim, J. Liu, H. Gliemann, C. Wöll, *Appl. Phys. Lett.* 2013, 103, 091903.
- M. L. Ohnsorg, C. K. Beaudoin, M. E. Anderson, *Langmuir* 2015, 31, 6114
- J. Lau, A. E. Trojniak, M. J. Maraugha, A. J. VanZanten, A. J. Osterbaan, A. C. Serino, M. L. Ohnsorg, K. M. Cheung, D. S. Ashby, P. S. Weiss, B. S. Dunn, M. E. Anderson, *Chem. Mater.* 2019, *31*, 8977.
- 26. A. Ulman, Chem. Rev. 1996, 96, 1533.
- C. Love, L. A. Estroff, J. K. Kriebel, R. G. Nuzzo, G. M. Whitesides, *Chem. Rev.* 2005, 105, 1103.
- 28. R. K. Smith, P. A. Lewis, P. S. Weiss, Prog. Surf. Sci. 2004, 75, 1.
- S. A. Claridge, W. Liao, J. C. Thomas, Y. Zhao, H. Cao, S. Cheunkar, A. C. Serino, A. A. Andrews, P. S. Weiss, *Chem. Soc. Rev.* 2013, 42, 2725.
- S. D. Evans, A. Ulman, K. E. Goppert-Berarducci, L. J. Gerenser, J. Am. Chem. Soc. 1991, 113, 5866.
- 31. Y. Xia, G. M. Whitesides, Annu. Rev. Mater. Sci. 1998, 28, 153.
- Y. Xia, G. M. Whitesides, Angew. Chem. Int. Ed. 1998, 37, 550.
- 33. A. Perl, D. Reinhoudt, J. Huskens, Adv. Mater. 2009, 21, 2257.
- S. J. Stranick, S. V. Atre, A. N. Parikhz, M. C. Woody, D. L. Allara, N. Winograd, P. S. Weiss, *Nanotechnology* 1996, 7, 438.
- S. J. Stranick, A. N. Parikh, Y.-T. Tao, D. L. Allara, P. S. Weiss, J. Phys. Chem. 1994, 98, 7636.

- H. Bayat, D. Tranchida, B. Song, W. Walczyk, E. Sperotto, H. Schönherr, *Langmuir* 2011, 27, 1353.
- C. D. Bain, J. Evall, G. M. Whitesides, J. Am. Chem. Soc. 1989, 111, 7155.
- 38. C. D. Bain, G. M. Whitesides, J. Am. Chem. Soc. 1989, 111, 7164.
- 39. P. E. Laibinis, G. M. Whitesides, J. Am. Chem. Soc. 1992, 114, 1990.
- A. A. Dameron, L. F. Charles, P. S. Weiss, J. Am. Chem. Soc. 2005, 127, 8697.
- 41. A. A. Dameron, J. R. Hampton, R. K. Smith, T. J. Mullen, S. D. Giullmore, P. S. Weiss, *Nano Lett.* **2005**, *5*, 1834.
- 42. M. Kim, J. N. Hohman, E. I. Morin, T. A. Daniel, P. S. Weiss, *J. Phys. Chem. A* **2009**, *113*, 3895.

SUPPORTING INFORMATION

Additional supporting information can be found online in the Supporting Information section at the end of this article.

How to cite this article: C. D. Fasana, F. G. Gonzalez, J. W. Wade, A. M. Weeks, B. D. Dhanapala, M. E. Anderson, *Aggregate* **2022**, *3*, e241. https://doi.org/10.1002/agt2.241